Biochemical and Biophysical Research Communications 480 (2016) 261–267

Contents lists available at ScienceDirect

Biochemical and Biophysical Research Communications

journal homepage: www.elsevier.com/locate/ybbrc

Crystal structure of the ADP-ribosylating component of BEC, the binary enterotoxin of *Clostridium perfringens*

Kazuki Kawahara [a, 1], Shinya Yonogi [b, c, 1], Ryota Munetomo [a], Hiroya Oki [a], Takuya Yoshida [a], Yuko Kumeda [b], Shigeaki Matsuda [c], Toshio Kodama [c], Tadayasu Ohkubo [a], Tetsuya Iida [c], Shota Nakamura [c, *]

[a] Graduate School of Pharmaceutical Sciences, Osaka University, Suita, Osaka, Japan
[b] Osaka Prefectural Institute of Public Health, Osaka, Osaka, Japan
[c] Research Institute for Microbial Diseases, Osaka University, Suita, Osaka, Japan

ARTICLE INFO

Article history:
Received 5 October 2016
Accepted 14 October 2016
Available online 15 October 2016

Keywords:
C. perfringens
Binary enterotoxin
Protein structure
X-ray crystallography

ABSTRACT

Binary enterotoxin of *Clostridium perfringens* (BEC), consisting of the components BECa and BECb, was recently identified as a novel enterotoxin produced by *C. perfringens* that causes acute gastroenteritis in humans. Although the detailed mechanism of cell intoxication by BEC remains to be defined, BECa shows both NAD^+-glycohydrolase and actin ADP-ribosyltransferase activities in the presence of NAD^+. In this study, we determined the first crystal structure of BECa in its apo-state and in complex with NADH. The structure of BECa shows striking resemblance with other binary actin ADP-ribosylating toxins (ADPRTs), especially in terms of its overall protein fold and mechanisms of substrate recognition. We present a detailed picture of interactions between BECa and NADH, including bound water molecules located near the C1′-N glycosidic bond of NADH and the catalytically important ADP-ribosylating turn-turn (ARTT) loop. We observed that the conformational rearrangement of the ARTT loop, possibly triggered by a conformational change involving a conserved tyrosine residue coupled with substrate binding, plays a crucial role in catalysis by properly positioning a catalytic glutamate residue in the E-X-E motif of the ARTT loop in contact with the nucleophile. Our results for BECa provide insight into the common catalytic mechanism of the family of binary actin ADPRTs.

1. Introduction

Clostridium perfringens is a well-known causative agent of various animal and human diseases, such as histotoxic and enteric infections, resulting from an ability of the organism to produce at least 17 different toxins reported to date [1,2]. The types and combinations of expressed toxins discovered are still increasing and expanding the known pathogenic consequences of *C. perfringens* infection [3–5]. The four major classical toxins, alpha, beta, epsilon, and iota toxins, classify *C. perfringens* isolates into five toxin types (A to E) [6,7]. C. *perfringens* enterotoxin (CPE) predominantly produced by *C. perfringens* type A isolates in sporulation is not included in the classification scheme, but is known as a main cause of human gastrointestinal illnesses, including food-borne gastroenteritis, antibiotic-associated diarrhea, and sporadic diarrhea [1–3]. In outbreaks of food-borne gastroenteritis due to *C. perfringens,* it is therefore important to detect CPE in patient fecal specimens and examine CPE production of *C. perfringens* isolates.

Recently, two food-borne gastroenteritis outbreaks occurred in Japan, which were caused by CPE-negative *C. perfringens* type-A isolates [5]. A novel enterotoxin, designated as binary enterotoxin of *C. perfringens* (BEC), distinct from CPE, was identified as the causative agent [5]. High-throughput genome sequencing revealed that BEC is composed of two proteins, BECa (~47 kDa) and BECb (~80 kDa), and has meaningful sequence homology with members of the binary ADP-ribosylating toxin (ADPRT)-family proteins, such as iota toxin from *C. perfringens* type E, C2 toxin from *C. botulinum*, *Clostridium difficile* toxin (CDT) from *C. difficile*, *Clostridium spiroforme* toxin (CST) from *C. spiroforme,* and vegetative insecticidal

* Corresponding author. Research Institute for Microbial Diseases, Osaka University, 3-1 Yamadaoka, Suita, Osaka 565-0871, Japan. Tel.: +81 6 6879 8318; fax: +81 6 6879 8372.
E-mail address: nshota@gen-info.osaka-u.ac.jp (S. Nakamura).
[1] Contributed equally.

http://dx.doi.org/10.1016/j.bbrc.2016.10.042

protein (VIP) from *Bacillus cereus* [5,8–12]. More recently, from another outbreak in Japan [13], the *C. perfringens* iota-like enterotoxin (CPILE), whose DNA sequence perfectly matched to BEC, was also identified as a possible source of CPE-negative *C. perfringens* type-A isolates, signifying the importance of understanding this novel enterotoxin in more detail.

Each binary ADPRT is composed of two separate components (an enzymatic A component and a cell-binding B component) [8,9], and mono-ADP-ribosylates globular actin during the cell-intoxication process, when both components work together [8–12]. Similar to cases observed with other binary ADPRTs, recombinantly expressed BEC has cytotoxic activity towards Vero cells, but only when both BECa and BECb are simultaneously administered [5]. Cytotoxicity resulting in cell rounding followed by cell lysis is primarily attributed to the actin ADP-ribosylating activity of BEC, which is clearly demonstrated by *in vitro* assays showing BECa has an actin ADP-ribosyltransferase activity in the presence of NAD^+ [5,8,12,13]. A sequence comparison showed that BECa possesses an aromatic residue-R/H, an E-X-E motif in the ADP-ribosylating turn-turn (ARTT) loop, and an S-T-S motif (second serine is threonine in BECa), which are highly conserved in the actin ADPRT family [14–18]. Based on these results, we concluded that the newly identified enterotoxin, BEC, is a binary enterotoxin that belongs to the actin ADPRT family.

In the present study, we determined the first crystal structure of BECa in its apo-state and in complex with NADH. The crystal structure of BECa showed remarkable similarity with other binary actin ADPRT-family members and reveals details of the substrate-binding mechanism of BECa, including implications for the mechanism underlying the molecular recognition of actin. Furthermore, we observed intriguing conformational variations of the catalytically important ARTT loop and several water molecules surrounding the substrate-binding pocket, both of which provide further insight into the precise functions and catalytic mechanisms of BECa.

2. Materials and methods

2.1. Crystallization

Expression and purification of BECa were performed as described previously [5]. Initial crystallization conditions were screened by sitting-drop vapor diffusion at 293 K, using the Crystal Screen 1 & 2 Formulation (Hampton Research). Crystallization drops were prepared by mixing 0.8 μL of protein solution (7.5 or 15 mg mL^{-1}) and 0.8 μL of reservoir solution and were equilibrated against 35 μL reservoir solutions. After several rounds of optimization, hexagonal crystals were obtained after 2 days from a mixture of 3 μL protein solution (7.5 mg mL^{-1}) and 2 μL reservoir solution consisting of 100 mM Tris-HCl (pH 8.8), 400 mM $MgCl_2 \cdot 6H_2O$, and 24% (w/v) polyethylene glycol 4000 at 293 K. A BECa-NADH crystal was grown by the co-crystallization method. The protein stock solution was diluted to 7.5 mg mL^{-1} and pre-incubated with the ligand NADH (10 mM) on ice. Using this solution, BECa-NADH was co-crystallized using the same conditions used for the BECa crystals. After optimization, hexagonal-shaped crystal of BECa-NADH was obtained in reservoir solution consisting of 100 mM Tris-HCl (pH 8.8), 450 mM $MgCl_2 \cdot 6H_2O$, and 23% (w/v) polyethylene glycol 4000 at 293 K.

2.2. Data collection and structure determination

Diffraction data from the BECa crystal were collected on an R-axis IV^{++} imaging plate detector using Cu-*Ka* X-rays from a Rigaku MicroMax-007 X-ray generator. The crystals were cryoprotected using reservoir solution and flash-cooled in a liquid nitrogen gas stream at 100 K. Data for the BECa crystal were processed with Crystal Clear software, version 1.3.5 (Rigaku) [19]. Diffraction data for the BECa-NADH complex crystal were collected at SPring-8 on beamline BL26B1 using a SaturnA200 CCD detector at 100 K. The data from the BECa-NADH crystal were processed with the

Table 1
Data collection and refinement statistics for the BECa and BECa-NADH structures.

	BECa	BECa-NADH
Data collection		
Wavelength (Å)	1.5418	1.0000
Space group	*I*222	*I*222
Unit cell dimensions		
a, *b*, *c* (Å)	69.85, 94.00, 121.06	70.34, 102.81, 125.03
α, β, γ (°)	90.0	90.0
Resolution range (Å)[a]	37.12–1.89 (1.96–1.89)	50.00–1.82 (1.85–1.82)
No. of unique reflections	31,752	40,199
Completeness (%)	98.4 (88.1)	99.8 (100.0)
Redundancy	9.5 (6.1)	7.0 (7.3)
$I/\sigma\langle I\rangle$	13.0 (4.2)	53.3 (10.8)
Overall B-factor from Wilson plot ($Å^2$)	23.5	22.7
R_{merge}[b]	0.095 (0.426)	0.073 (0.377)
Refinement		
R_{work}/R_{free}[c]	0.207/0.257	0.179/0.218
RMSD from ideal values		
Bond length (Å)	0.009	0.007
Bond angles (°)	1.034	0.827
Overall B-factors ($Å^2$)	30.0	31.0
Ramachandran plot statistics (%)		
Most favored	97.3	97.8
Allowed	2.7	2.2
Disallowed	0.0	0.0

[a] The values shown in parentheses are for the highest resolution shell.
[b] $R_{merge} = \sum_{hkl}\sum_i |I_i(hkl) - \langle I(hkl)\rangle| / \sum_{hkl}\sum_i I_i(hkl)$, where $I_i(hkl)$ is the intensity of the *i* th measurement of an equivalent reflection and $\langle I(hkl)\rangle$ is the mean intensity for multiply recorded reflections.
[c] $R_{work} = \sum||F_o|-|F_c|| / \sum|F_o|$, where F_o and F_c are the calculated protein structure factors from the atomic model. R_{free} is calculated based on 10% randomly selected reflections not included in the calculation of the R_{work}.

HKL2000 package [20]. The BECa structure was determined by the molecular replacement method using the Phaser program from the PHENIX suite [21]. As a search model, the iota toxin Ia structure in complex with NADPH (PDB code: 1gir) was used. The final model building was performed using the COOT program and refined with the phenix.refine program from PHENIX suite [21,22]. The structure of the BECa-NADH complex was determined by the molecular replacement method using the structure of apo-BECa, and was refined using the same protocol that was used for BECa. The geometries of the final models were analyzed with MolProbity [23]. All data-collection and refinement statistics are given in Table 1. The atomic coordinates and structural factors (code 5h03 for BECa and 5h04 for BECa-NADH) have been deposited in the Worldwide Protein Data Bank.

3. Results and discussion

3.1. Overall structure of BECa

We determined the crystal structure of BECa by a molecular replacement method utilizing the reported structure (PDB code: 1gir) of an enzymatic component of iota toxin (Ia) of *C. perfringens* (Table 1). The crystal structure of BECa showed structurally homologous N- and C-terminal domains, comprising residues 3–209 and residues 217–419, respectively (Fig. 1A). Both domains were linked by a short loop consisting of residues 210–216. Each core domain adopted a mixed α/β protein fold, formed mainly by perpendicular packing of a 5-stranded mixed β-sheet against a 3-stranded antiparallel β-sheet. The β-sheet was surrounded by four consecutive α-helices and one additional α-helix, forming a central cleft characteristic of all members of the actin ADPRT family [9,17,24].

Sequence alignment revealed that BECa shares sequence homology with an enzymatic component of binary actin ADPRTs, such as Ia from *C. perfringens* (44% identity), CDTa from *C. difficile* (43% identity), Sa from *C. spiroforme* (42% identity), Isp2b from *B. laterosporus* (34% identity), VIP2 from *B. thuringiensis* (28% identity), and C2-I from *C. botulinum* (29% identity) [5]. Despite the low-to-moderate sequence identity (28%–44%), structural superimpositions among these toxins showed remarkable similarity in their overall protein folds, indicating structural conservation of the ADPRT family (Fig. 1B) [14,15,24,25]. When we mapped the sequence conservation onto the molecular surface (Fig. 1C), however, most surface residues were not well conserved, except for one region at the central cleft of the C-terminal domain. At the cleft, several residues, known to be critical for substrate (NAD^+)

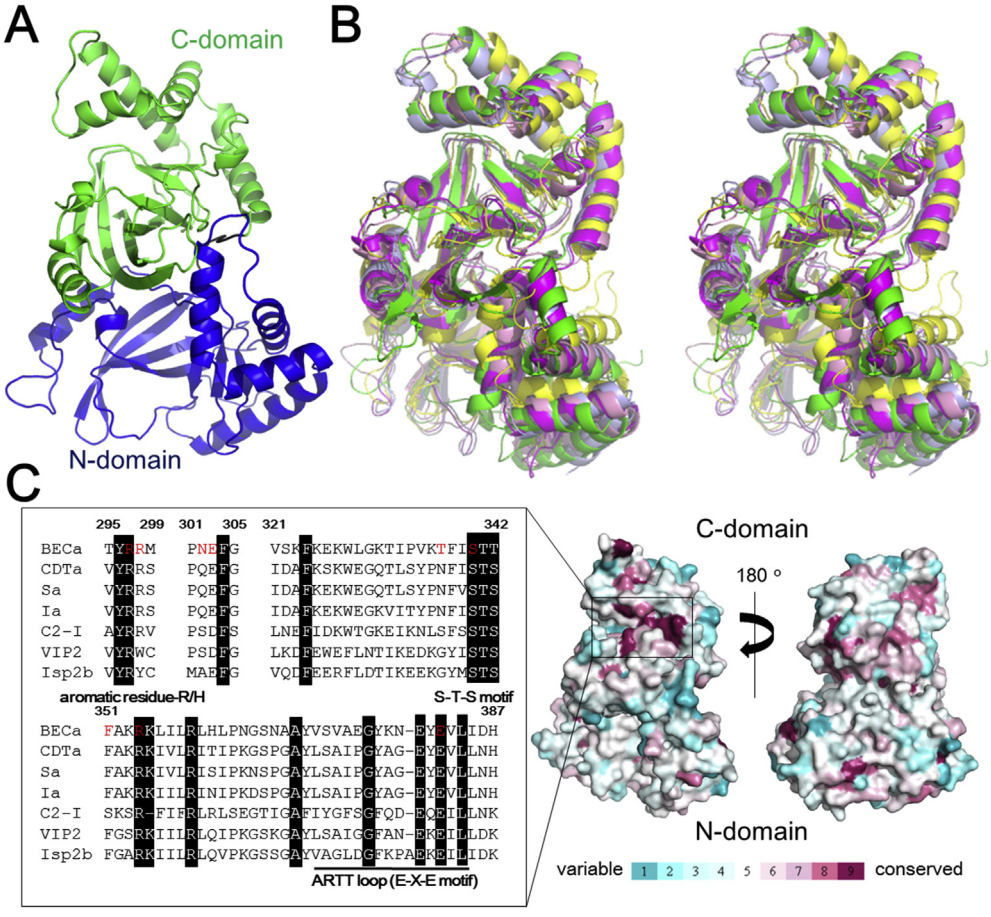

Fig. 1. Overall structure of BECa from *C. perfringens*. (A) The crystal structure of BECa represented by cartoon model. The homologous N- and C-terminal domains are colored in blue and green, respectively. (B) Structural comparison between BECa and other actin ADPRTs. The structure of BECa (pink) is superimposed with other reported structures of actin ADPRTs, including CDTa (PDB code: 2wn8) from *C. difficile* (light blue), Ia (PDB code: 1giq) from *C. perfringens* (magenta), VIP2 (PDB code: 1qs1) from *B. cereus* (yellow), and C2-I (PDB code: 2j3z) from *C. botulinum* (green). (C) Molecular surface representation of BECa colored by *Consurf* sequence conservation [30]. Each residue position is colored according to the degree of conservation using the color-coding bar. Sequence-alignment results for the substrate-binding site of actin ADPRTs (BECa from *C. perfringens*, CDTa from *C. difficile*, Ia from *C. perfringens*, Sa from *B. spiroforme*, Isp2b from *B. laterosporus*, VIP2 from *B. cereus*, and C2-I from *C. botulinum*) are also shown. Strictly conserved residues are highlighted as white letters. The residues critical for substrate recognition of BECa-NADH complex (Fig. 2) is colored in red. (For interpretation of the references to colour in this figure legend, the reader is referred to the web version of this article.)

recognition and catalytic behavior, were outstandingly conserved (Fig. 1C) [17]. While the residues at the central cleft of the C-terminal domain were highly conserved, those at the N-terminal domain were not, showing some asymmetry in their molecular surface characteristics. It has been reported that the N-terminal domain is not only responsible for the interaction with the cell-binding component of the binary ADPRTs, but also critical for the actin recognition, showing a multimodal function of the N-terminal domain [5,8,17]. These structural and sequence comparisons thus suggested that the enzymatic component of binary ADPRTs may have initially arisen as a consequence of duplication of an ancestral ADP-ribosyltransferase gene, but could have evolved differentially to obtain additional functions, including substrate recognition and translocation into target cells.

3.2. Substrate-recognition mechanisms of BECa

We recently demonstrated that BECa ADP-ribosylates globular actin by catalyzing the transfer of the ADP-ribose moiety of NAD^+ to actin [5]. Concomitantly the enzymatic component of binary actin ADPRTs has an NADase activity that typically renders structural determination of ADPRT-NAD^+ complexes difficult [13,15]. Therefore, in this study, we determined the structure of BECa in complex with NADH by co-crystallization method (Fig. 2).

In the complex, the NADH molecule bound at the central cleft of the C-terminal domain of BECa without forcing a significant conformational change (Fig. 2A). The NADH molecule adopted a highly folded conformation (Fig. 2B), potentially important for oxocarbenium ion formation [26], with its nicotinamide moiety deeply embedded into the hydrophobic pocket surrounded by the residues, Phe351 and Ile348 (Fig. 2C). The carboxamide group of the nicotinamide moiety formed hydrogen bonds with the carbonyl and amide groups of Arg298, which further stabilized the nicotinamide conformation. At the molecular surface, the ADP-ribose moiety of NADH was tightly associated with BECa through direct or water-mediated hydrogen bonding interactions, as observed for other binary ADPRTs. These interactions involved residues Arg297, Asn302, Glu303, Thr337, Arg354, and Glu382 of BECa, which correspond to residues Arg295, Gln300, Glu301, Asn335, Arg352, and Glu380 of its closest homologue Ia from *C. perfringens* in the recently reported structure of the Ia-NAD^+-actin ternary complex [18]. Additional interactions between Asn256 and the NADH as well as between S340 and the NADH were also observed for BECa, but not for Ia, although the corresponding residues Asn255 and Ser338, respectively of Ia was located a considerable distance away (Fig. 2C). The sequence comparison indicated that the manner of substrate recognition observed here (and hence the catalytic mechanism) is widely conserved among the family of binary actin

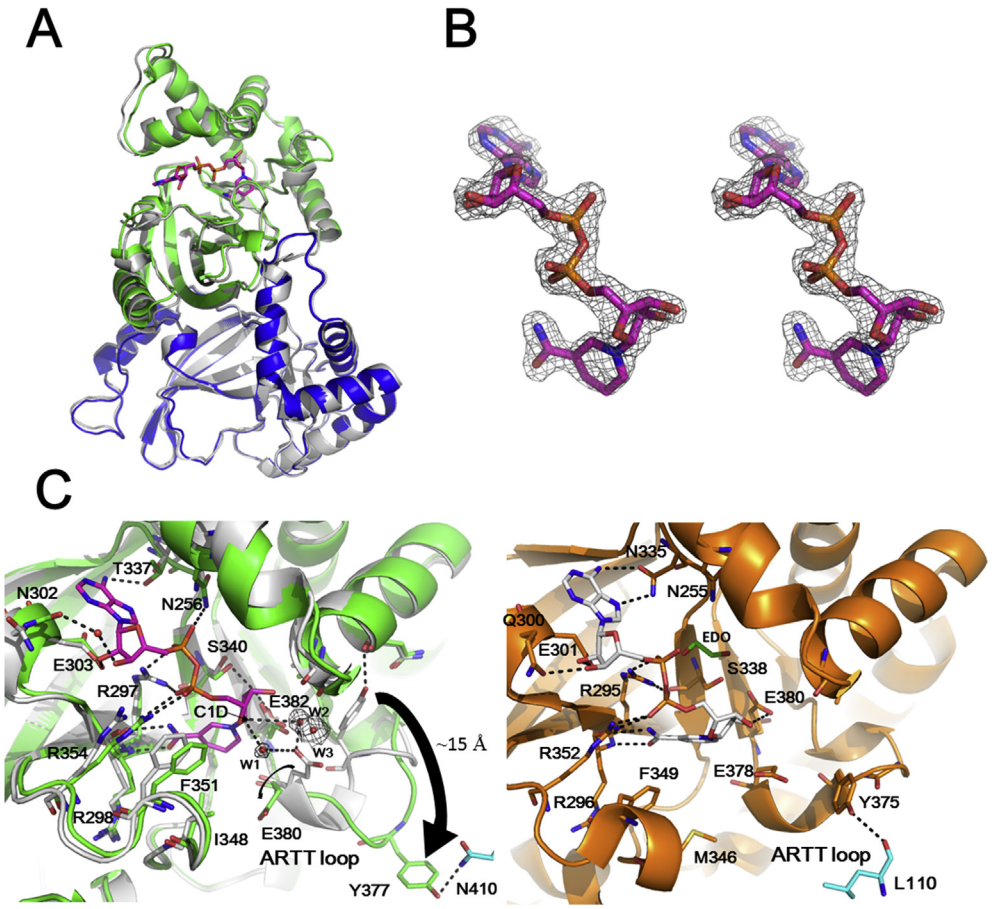

Fig. 2. Overall structure of BECa in complex with NADH. (A) Superimposition of the BECa-NADH complex (green for the C-terminal domain and blue for the N-terminal domain) onto the apo-state of BECa (white). (B) Stereo-view of the $2mF_o$-DF_c electron density map for NADH molecule contoured at 1.5 σ. (C) Left panel, superposed view of the substrate-binding site of the BECa-NADH complex (green) and BECa in the apo-state (white). Key residues: N256, R297, R298, N302, E303, T337, S340, I348, F351, R354, and E382, involved in NADH recognition; E380 and Y377, belonging to the ARTT loop of BECa. N410 of BECa from the symmetry-related molecule is colored light blue. The $2mF_o$-DF_c electron density for the water molecules (W1, W2, and W3) contoured at 1.0 σ is also shown. Right panel, detailed view of the substrate-binding site of Ia (orange) of the Ia-NAD^+-actin ternary complex (PDB code: 4h03). Key residues: R295, R296, Q300, E301, N335, M346, F349, R352, and E376, involved in NAD^+ recognition; E378 and Y375, belonging to the ARTT loop of Ia. L110 of actin is colored light blue. (For interpretation of the references to colour in this figure legend, the reader is referred to the web version of this article.)

ADPRTs (Fig. 1C).

To date, several water molecules have been found in the NAD^+-binding pocket in the reported structures of actin ADPRT-substrate complex; however, to our knowledge, no water molecule or possible nucleophile have been observed near the catalytic center (C1D) or around the nicotinamide mononucleotide (NMN) ring of NAD^+. Intriguingly, we observed electron densities for at least three water molecules (W1, W2, and W3) in close proximity (<5.1 Å) to the C1′-N glycosidic bond of the NADH molecule, one of which (W1) was located at a distance of 3.3 Å away from the C1D atom of NADH (Fig. 2C). This location might enable the water molecule to initiate a nucleophilic attack on the catalytic center of NAD^+, resulting in NADase reaction. Despite the substantial structural similarity, no water molecule was modelled at the corresponding region of the Ia-NAD^+-actin ternary complex. Instead, it is noteworthy that ethylene glycol (EDO) molecules, which could potentially interfere with water molecules in the crystal, were found at the NAD^+-binding site [18].

Despite the tremendous efforts, the precise mechanisms facilitating the NADase and ADP-ribosyltransferase activities of actin ADPRTs are still debated [24,27]. Previous mutational studies of several of the actin ADPRT family toxins showed that the well conserved E-X-E motif (Glu380-Y381-Glu382 in BECa) in the ARTT loop plays important roles in substrate recognition and enzymatic activities [28]. Of the two glutamate residues, the latter glutamate (Glu382 in BECa) forms hydrogen bond with the O2′ hydroxyl of the nicotinamide ribose, which may stabilize the oxocarbenium ion that is presumably produced when nicotinamide is cleaved off from NAD^+ [24]. Mutational studies for ADPRTs also showed that the former glutamate residue (Glu380 in BECa) acts in deprotonation of Arg177 of actin and/or water molecules to promote nucleophilic attack on the catalytic center of NAD^+ [18]. In our BECa-NADH complex, although it located close to the NMN ring, the Glu380 residue is located 4.9 Å, 7.0 Å and 6.9 Å away from the above-mentioned water molecules W1, W2, and W3, respectively (Fig. 2C). Nevertheless, as demonstrated by the superposition between the apo-BECa and BECa-NADH structures (Fig. 2C), Glu380 could be positioned 3.7 Å and 2.2 Å away from water molecules W1 and W2, respectively. The overall structures of both the apo and complex form of BECa were essentially similar with RMSD value of 0.55 Å; however, ARTT loop conformation was quite different, especially at Tyr377. The tyrosine residue interacted with the backbone carbonyl of Asn245 in its apo-state, but protruded toward the solvent region in the BECa-NADH complex, interacting with Asn410 of the symmetry-related BECa molecule (Fig. 2C). This suggests its intrinsically flexible nature of the ARTT loop, facilitating protein-protein interactions, in this case molecular packing interactions in the crystal. The difference (~15 Å) in position of the tyrosine residue plausibly affected the conformational state of the ARTT loop, by which the spatial positioning of Glu380 was apparently affected. Remarkably, the corresponding tyrosine residue also protruded outward to interact with the actin molecule in the Ia-NAD^+-actin

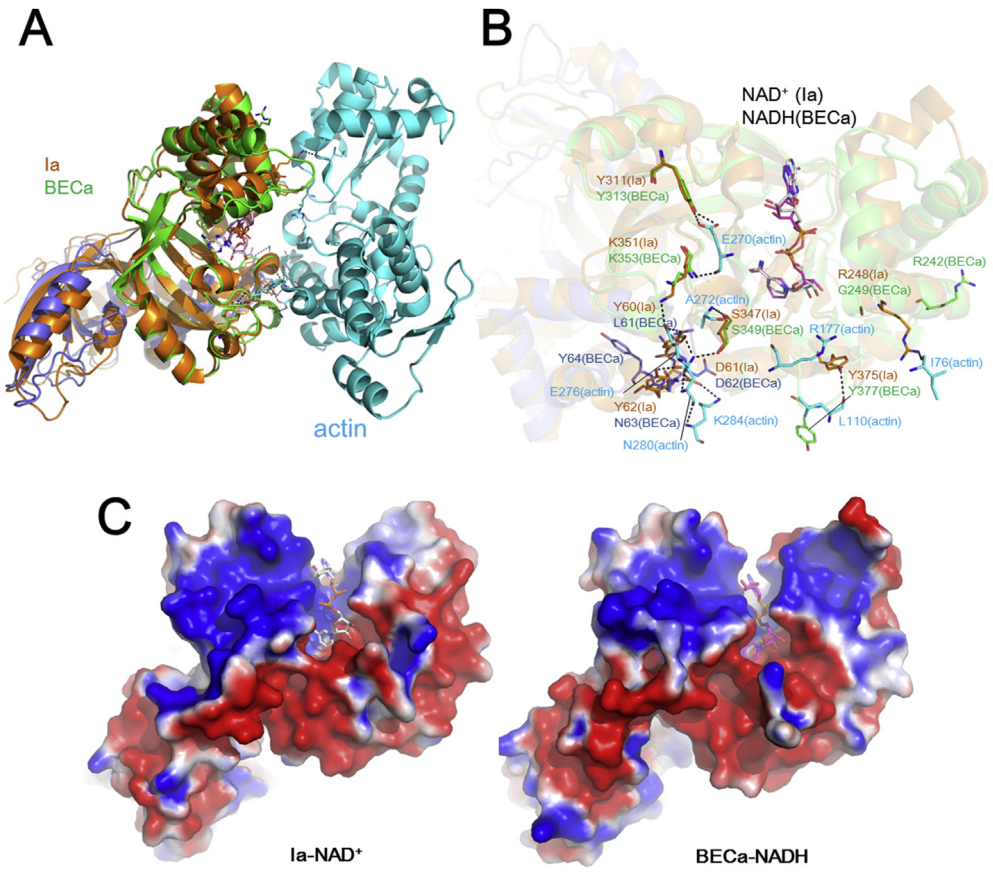

Fig. 3. Structural model of the BECa-NADH-actin complex. (A) Structural superimposition of the BECa-NADH complex onto the Ia subunit of the Ia-NAD^+-actin ternary complex (PDB code: 4h03). In the BECa-NADH complex, the N- and C-terminal domains are colored in green and blue, respectively. In the Ia-NAD^+-actin ternary complex, Ia and actin are colored in orange and light blue. Key residues involved in the interaction between actin and Ia are shown in a stick model. (B) Detailed view of binding interface of the Ia-NAD^+-actin ternary complex. Key residues responsible for the interaction are shown in a stick model. (C) The electrostatic surface potentials of the Ia-NAD^+ complex from the Ia-NAD^+-actin ternary complex (left panel) and the BECa-NADH complex (right panel). (For interpretation of the references to colour in this figure legend, the reader is referred to the web version of this article.)

ternary complex [18], indicating that actin binding could promote significant conformational changes in the ARTT loop, further reinforcing its critical role in protein-protein interactions (Fig. 2C). Together with the fact that the aromatic residue (Tyr377 in BECa) in the ARTT loop is widely conserved among binary actin ADPRTs, these observations indicated the possibility of the tyrosine residue playing a pivotal role in the conformational rearrangement of the ARTT loop, which is prerequisite for proper positioning of the conserved glutamate residues in the E-X-E motif for catalytic activity.

3.3. Implication for the BECa-actin interaction

To gain structural insight into actin recognition of BECa, we built a model of the BECa-NADH-actin ternary complex by superposing the BECa-NADH complex onto the Ia subunit of Ia-NAD^+-actin ternary complex (Fig. 3). In the Ia-NAD^+-actin ternary complex, amino acid residues Ile76, Leu110, Glu270, Ala272, Glu276, Asn280, Lys284 of actin were recognized by Ia (Fig. 3B). Of the seven interacting residues in actin, the structural superposition demonstrated that almost all of these residues, except for Ile76, potentially interacted with BECa with almost the same set of interacting residues (Asp62, Tyr313, Ser349, Lys353, and Tyr377 of BECa correspond to Asp61, Tyr311, Ser347, Lys351, and Tyr375 of Ia), suggesting the mechanistic similarity between BECa and Ia in actin recognition. However, it should be pointed out that Arg248 of Ia, which interacted with the backbone carbonyl of Ile76 of actin, is not conserved and is substituted to glycine in BECa, and two tyrosine residues in Ia (Tyr60 and Tyr62) that stabilize the Ia-actin Glu276 interaction, were substituted to Leu61 and Asn63, respectively, in BECa. These differences in amino acid conservation indicated the lower affinity of BECa than Ia for actin binding, due to the fact that previous mutational studies showed that the three residues (Arg248, Tyr60, and Tyr62) play important roles for its ADP-ribosyltransferase activity [16]. However, it is interesting to note that the sequence alignment showed that Arg248, Tyr60, and Tyr62, which are important for actin recognition by Ia, are not strictly conserved among the actin ADPRT family members [16], indicating the possibility for some variations in protein-substrate recognition among the family toxins. In this context, we found that BECa Arg242 (located close to Ia Arg248) potentially contacts actin Ile76, and BECa residues Asn63 and Tyr64 (positioned closely to Ia residues Tyr60 and Tyr62, respectively) likely interact with actin Glu276 (Fig. 3B). Furthermore, as shown in Fig. 3C, BECa and Ia show similar electrostatic surface potential charge distribution at the proposed enzyme-actin interface, which is also critical in ADPRT recognition of protein substrates [29]. These results support the existence of similar substrate-recognition mechanisms. Our structural-modeling analysis also suggested that Arg177 of actin is located near the NMN ring of NADH and therefore might be targeted by BECa, as occurs with other actin ADPRTs.

In conclusion, we determined an enzymatic component of the newly found BECa protein, both in its apo-state and in complex with NADH. Despite its limited sequence identity with that of other binary actin ADPRT family toxins, the structure and substrate-recognition mechanisms of BECa are almost the same as other ADPRT family toxins. While the strict conservation of residues at the substrate-binding pocket in the C-terminal domain is critical for its catalytic activity, conservation of the amino acid residues spanning the molecular surface, especially within the N-terminal domain, is relatively low. These findings suggest that differences in affinity and selectivity occur within the binary actin ADPRT family, which facilitates interactions between its enzymatic and cell-binding component as well as with various cognate host cell molecules enabling internalization and subsequent pathogenesis, the mechanism of which is still not fully understood and thus awaits future investigations.

Acknowledgement

The synchrotron X-ray experiments were performed with the approval of the SPring-8 Program Advisory Committee (2014A1344, 2014B1234). This study was supported by Grant-in-Aid for Young Scientists (B) from the Ministry of Education, Culture, Sports, Science and Technology of Japan (MEXT) (93018810).

Transparency document

Transparency document related to this article can be found online at http://dx.doi.org/10.1016/j.bbrc.2016.10.042.

References

[1] J.C. Freedman, A. Shrestha, B.A. McClane, Clostridium perfringens enterotoxin: action, genetics, and translational applications, Toxins Basel 8 (2016) pii: E73.
[2] J.C. Freedman, J.R. Theoret, J.A. Wisniewski, et al., Clostridium perfringens type A-E toxin plasmids, Res. Microbiol. 166 (2015) 264–279.
[3] J. Li, V. Adams, T.L. Bannam, et al., Toxin plasmids of Clostridium perfringens, Microbiol. Mol. Biol. Rev. 77 (2013) 208–233.
[4] A.L. Keyburn, J.D. Boyce, P. Vaz, et al., NetB, a new toxin that is associated with avian necrotic enteritis caused by Clostridium perfringens, PLoS Pathog. 8 (2008) e26.
[5] S. Yonogi, S. Matsuda, T. Kawai, et al., BEC, a novel enterotoxin of Clostridium perfringens found in human clinical isolates from acute gastroenteritis outbreaks, Infect. Immun. 82 (2014) 2390–2399.
[6] J.G. Smedley 3rd, D.J. Fisher, S. Sayeed, et al., The enteric toxins of Clostridium perfringens, Rev. Physiol. Biochem. Pharmacol. 152 (2004) 183–204.
[7] M.R. Popoff, P. Bouvet, Clostridial toxins, Future Microbiol. 4 (2009) 1021–1064.
[8] B.G. Stiles, K. Pradhan, J.M. Fleming, et al., Clostridium and bacillus binary enterotoxins: bad for the bowels, and eukaryotic being, Toxins Basel 6 (2014) 2626–2656.
[9] H. Barth, K. Aktories, M.R. Popoff, et al., Binary bacterial toxins: biochemistry, biology, and applications of common Clostridium and Bacillus proteins, Microbiol. Mol. Biol. Rev. 68 (2004) 373–402.
[10] M.R. Popoff, F.W. Milward, B. Bancillon, et al., Purification of the Clostridium spiroforme binary toxin and activity of the toxin on HEp-2 cells, Infect. Immun. 57 (1989) 2462–2469.
[11] M. Roeder, E.M. Nestorovich, V.A. Karginov, et al., Tailored cyclodextrin pore blocker protects mammalian cells from clostridium difficile binary toxin CDT, Toxins Basel 6 (2014) 2097–2114.
[12] H. Barth, R. Roebling, M. Fritz, et al., The binary Clostridium botulinum C2 toxin as a protein delivery system: identification of the minimal protein region necessary for interaction of toxin components, J. Biol. Chem. 277 (2002) 5074–5081.
[13] D. Irikura, C. Monma, Y. Suzuki, et al., Identification and characterization of a new enterotoxin produced by Clostridium perfringens isolated from food poisoning outbreaks, PLoS One 10 (2015) e0138183.
[14] A. Sundriyal, A.K. Roberts, C.C. Shone, et al., Structural basis for substrate recognition in the enzymatic component of ADP-ribosyltransferase toxin CDTa from Clostridium difficile, J. Biol. Chem. 284 (2009) 28713–28719.
[15] H. Tsuge, M. Nagahama, H. Nishimura, et al., Crystal structure and site-directed mutagenesis of enzymatic components from Clostridium perfringens iota-toxin, J. Mol. Biol. 325 (2003) 471–483.
[16] H. Tsuge, M. Nagahama, M. Oda, et al., Structural basis of actin recognition and arginine ADP-ribosylation by Clostridium perfringens iota-toxin, Proc. Natl. Acad. Sci. U. S. A. 105 (2008) 7399–7404.
[17] J. Sakurai, M. Nagahama, M. Oda, et al., Clostridium perfringens iota-toxin: structure and function, Toxins Basel 1 (2009) 208–228.
[18] T. Tsurumura, Y. Tsumori, H. Qiu, et al., Arginine ADP-ribosylation mechanism based on structural snapshots of iota-toxin and actin complex, Proc. Natl. Acad. Sci. U. S. A. 110 (2013) 4267–4272.
[19] J.W. Pflugrath, The finer things in X-ray diffraction data collection, Acta Crystallogr. D. Biol. Crystallogr. 55 (1999) 1718–1725.
[20] Z. Otwinowski, W. Minor, Processing of X-ray diffraction data collected in oscillation mode, Methods Enzymol. 276 (1997) 307–326.
[21] P.D. Adams, P.V. Afonine, G. Bunkóczi, et al., PHENIX: a comprehensive Python-based system for macromolecular structure solution, Acta Crystallogr. D. Biol. Crystallogr. 66 (2010) 213–221.
[22] P. Emsley, B. Lohkamp, W.G. Scott, et al., Features and development of Coot, Acta Crystallogr. D. Biol. Crystallogr. 66 (2010) 486–501.
[23] V.B. Chen, W.B. Arendall 3rd, J.J. Headd, et al., MolProbity: all-atom structure validation for macromolecular crystallography, Acta Crystallogr. D. Biol. Crystallogr. 66 (2010) 12–21.

[24] S. Han, J.A. Craig, C.D. Putnam, et al., Evolution and mechanism from structures of an ADP-ribosylating toxin and NAD complex, Nat. Struct. Biol. 6 (1999) 932–936.
[25] C. Schleberger, H. Hochmann, H. Barth, et al., Structure and action of the binary C2 toxin from Clostridium botulinum, J. Mol. Biol. 364 (2006) 705–715.
[26] C.E. Bell, T.O. Yeates, D. Eisenberg, Unusual conformation of nicotinamide adenine dinucleotide (NAD) bound to diphtheria toxin: a comparison with NAD bound to the oxidoreductase enzymes, Protein Sci. 6 (1997) 2084–2096.
[27] N.C. Simon, K. Aktories, J.T. Barbieri, Novel bacterial ADP-ribosylating toxins: structure and function, Nat. Rev. Microbiol. 12 (2014) 599–611.
[28] S. Han, J.A. Tainer, The ARTT motif and a unified structural understanding of substrate recognition in ADP-ribosylating bacterial toxins and eukaryotic ADP-ribosyltransferases, Int. J. Med. Microbiol. 291 (2002) 523–529.
[29] J. Sun, A.W. Maresso, J.J. Kim, et al., How bacterial ADP-ribosylating toxins recognize substrates, Nat. Struct. Mol. Biol. 11 (2004) 868–876.
[30] H. Ashkenazy, S. Abadi, E. Martz, et al., ConSurf 2016: an improved methodology to estimate and visualize evolutionary conservation in macromolecules, Nucleic Acids Res. 44 (W1) (2016) W344–W350.